Effects of non-toxic zinc exposure on human epidermal keratinocytes

Eszter Emri[1], Edit Miko[1], Péter Bai[2,5,6], Gábor Boros[1], Georgina Nagy[1,3], Dávid Rózsa[1], Tamás Juhász[4], Csaba Hegedűs[1], Irén Horkay[1], Éva Remenyik[1*], Gabriella Emri[1]

Departments of [1]Dermatology, [2]Medical Chemistry, [3]Dermatological Allergology, and [4]Anatomy, Histology, and Embryology, Faculty of Medicine, University of Debrecen, 4032, Debrecen, Hungary

[5]Research Center for Molecular Medicine, University of Debrecen, Debrecen, 4032, Hungary

[6]MTA-DE Lendület Laboratory of Cellular Metabolism Research Group, of the Hungarian Academy of Sciences 4032, Debrecen, Hungary

* All correspondence should be sent to:

Éva Remenyik, M.D., D.Sc.

Department of Dermatology

Faculty of Medicine, University of Debrecen

Nagyerdei krt. 98. H-4032, Debrecen, Hungary

Ph.: +36-52-411-600; F.: +36-52-414-632; E-mail: remenyik@med.unideb.hu

Abstract

Zinc is an essential microelement; its importance to skin is shown by severe skin symptoms in hereditary or acquired zinc deficiency, by the improvement of several skin conditions using systemic or topical zinc preparations and by the induced intracellular zinc release upon UVB exposure, which is the main harmful environmental factor to skin. Understanding the molecular background of the role of zinc in skin may help to gain insight into the pathology of skin disorders and to provide evidence for the therapeutic usefulness of zinc supplementation. Herein, we studied the effect of zinc chloride ($ZnCl_2$) exposure on the function of HaCaT keratinocytes, and we found that a non-toxic elevation in the concentration of extracellular zinc (100 µM) facilitated cell proliferation and induced significant alterations in the mRNA expression of NOTCH1, IL8, and cyclooxygenase-2. In addition, we detected increased heme oxygenase-1 (HMOX1) expression and non-toxic generation of superoxide in the first 4 h. Regarding the effect on UVB-induced toxicity, although the level of cyclobutane pyrimidine dimers in keratinocytes pre-treated with zinc for 24 h was reduced 3 h after UVB irradiation, we found significantly enhanced superoxide generation 10 h after UVB exposure in the zinc pre-exposed cells. The overall survival was unaffected; however, there was a decrease in the percentage of early apoptotic cells and an increase in the percentage of late apoptotic plus necrotic cells.

Our results suggest that exposure of human keratinocytes to non-toxic concentrations of $ZnCl_2$ impacts gene expression, cell proliferation and the response to environmental stress in skin. It would be important to further examine the role of zinc in skin and to further clarify if this issue can affect our thinking about the pathogenesis of skin diseases.

1. Introduction

Zinc is an essential microelement, and its importance in skin is shown by the severe skin symptoms of hereditary or acquired zinc deficiency, including erythaematous rashes, scaly plaques, and ulcers at orifices and acra [1, 2], and by the ability of systemic or topical zinc preparations to improve hair loss, acne and several inflammatory skin conditions [3].

Zinc content of the body is associated with skin by approximately 9%, primarily with the epidermis (50–70 µg g^{-1} dry weight) [4, 5], and 50% of the available zinc is localised to the cytoplasm, while 30–40% is localised in the nucleus, and the remainder is associated with the plasma membrane [6]. The cellular level and distribution of zinc is tightly controlled by zinc importers and transporters [7]. The metallothionein (MT)/thionein couple sequester or release zinc depending on the local redox state, thereby influencing the function of numerous proteins, transcription factors and enzymes [8]. An imbalance in the MT protein level can be detected in different skin cancers, in squamous cell carcinoma and in malignant melanoma [9, 10]. Indeed, the prevalence of genes encoding zinc proteins is estimated to be over 3% of the 32,000 identified genes [3]. According to Schwartz et al., over 300 zinc-dependent enzymes have been identified and characterised [11]. A close relation between redox homeostasis and the regulation of different protein functions by zinc can provide an important, fine-tuned control mechanism in the cell, but this process has been evidenced biochemically and has not been well studied in biological systems. On the other hand, zinc exposure of skin keratinocytes via cosmetic products, sunscreens and dermatological topical treatment occurs daily [4, 12]. The toxic effects of zinc pirithion and zinc oxide on the epidermis have been demonstrated [13, 14]; however, it is not known whether nontoxic zinc exposure can impact the physiological functions of keratinocytes or influence the effects of other environmental factors.

Ultraviolet light B (UVB) irradiation of human skin is known to induce pathophysiological processes such as oxidative stress and inflammation and is regarded as the main pathogenic factor of skin cancer development. UVB causes skin cell damage directly by inducing the production of cyclobutane pyrimidine dimers (CPDs) and indirectly by triggering the production of reactive species and interfering with cellular redox homeostasis. Importantly, rapid intracellular elevation of zinc levels occurs in keratinocytes after UVB irradiation [15, 16], and the level of MT is higher in the epidermis after acute UV exposure, while the skin of MT knockout mice is more susceptible to UVB [17]. Previously, it was found that solar (i.e., mixed) UV irradiation of keratinocytes exposed to zinc chloride (ZnCl$_2$) enhances cell survival and is able to reduce the immediate DNA damage [18, 19] and DNA fragmentation after exposure [20]. In

this study, we aimed to obtain further experimental evidence on the effect of Zn (II) exposure on human keratinocyte function in conventional culture and under stressed conditions using UVB irradiation, the main environmental harmful factor to skin.

2. Materials and methods

2.1. Cell culture, UVB-irradiation apparatus, and ZnCl₂ treatment

HaCaT human keratinocytes were obtained from ATCC and maintained in high-glucose DMEM (PAA, Traun, Austria) supplemented with 10% foetal bovine serum ((FBS) Lonza, Verviers, Belgium), 2 mM L-glutamine (PAA, Traun, Austria), 100 U/mL penicillin G, 0.1 mg/mL streptomycin sulphate, and 0.25 μg/mL amphotericin B (Sigma-Aldrich, St. Louis, MO, USA) in an atmosphere of 5% CO_2 at 37°C. In the UV irradiation experiments, the culture medium was replaced with sufficient phosphate-buffered saline (PBS) (DPBS, Lonza, Verviers, Belgium) to avoid dehydration. The cells were then exposed to UVB (20 mJ/cm^2) using a TL20W/12 RS broadband, filtered UVB lamp (Philips, Germany), which had an emission spectrum of 280–370 nm, with a peak at 312 nm. The UV intensity was controlled with a UV light meter (UVP Inc., San Gabriel, USA). The original medium was replaced after treatment. A 0.1-M stock solution of $ZnCl_2$ (Sigma-Aldrich, St. Louis, MO, USA) was prepared in deionised water and sterilised with a 0.2-μm sterile filter. A working concentration of 100 μM (unless stated otherwise) was selected according to previous reports [20].

2.2. Apoptosis assay

Cells were pre-treated with $ZnCl_2$ for 24 h and then exposed to UVB. Afterward, apoptosis was measured 24 h after UVB exposure. Harvested cells (5 x 10^5) were washed in ice-cold PBS and stained with Annexin V and propidium iodide (PI) using the Vybrant apoptosis assay Kit (Invitrogen, Eugene, Oregon, USA) according to the manufacturer's protocol. The stained cells were analysed by flow cytometry (CyFlow® Space, Partec, Canterbury, United Kingdom) using UV/488 nm dual-excitation, measuring the fluorescence emission at 530 and 575 nm. Annexin V$^-$PI$^-$ cells were identified as viable cells, Annexin V$^+$PI$^-$ cells were identified as early apoptotic cells, and the sum of the Annexin V$^+$PI$^+$ and Annexin V$^-$PI$^+$ cells was identified as late apoptotic plus necrotic cells.

2.3. Cell proliferation

Cells were treated with 50 or 100 µM $ZnCl_2$ for 72 h, and cell proliferation was measured using the EZ4U assay (Biomedica, Vienna, Austria) according to the manufacturer's instructions. The optical density (OD) was determined at 450 nm using an Anthos 2020 microplate reader (Biochrom Ltd., Cambridge, UK).

2.4. Cyclobutane pyrimidine dimer (CPD)-ELISA

Cells were treated with $ZnCl_2$ for 24 h and/or UVB irradiated, and genomic DNA was purified 0, 1, 3, 6, and 24 h after UVB exposure using a QIAamp Blood Kit (Qiagen, Hilden, Germany). Ninety-six-well plates were coated with 0.003% protamine sulphate (Sigma-Aldrich, St. Louis, MO, USA) for 2 days at 37°C. To measure CPD lesions, genomic DNA was diluted to 0.2 µg/mL in PBS, denatured at 100°C for 10 min, and then chilled on ice for 15 min. The denatured DNA solution was transferred to plates pre-coated with protamine sulphate and dried overnight at 37°C. For blocking, the plates were washed four times with PBS-T (0.05% Tween-20 in PBS) and then incubated in 20% FBS for 30 min at 37°C. The wells were then washed four times with PBS-T and incubated with the primary CPD antibody (#TDM-2, Cosmo Bio Co. Ltd., Tokyo, Japan) at a 1:1000 dilution in PBS for 30 min at 37°C. The wells were then washed and incubated with the HRP-conjugated anti-mouse IgG secondary antibody (BioRad, Hercules, CA, USA) diluted 1:3000 in PBS for 30 min at 37°C. After incubation, the cells were washed four times with PBS-T and then once with citrate-phosphate buffer (pH 5.0). Following buffer removal, the wells were incubated with a substrate solution (o-phenylene diamine (Sigma-Aldrich, St Louis, MO, USA), H_2O_2, and citrate-phosphate buffer (pH 5.0)) for 10 min at 37°C, at which time the enzyme reaction was stopped with 2 M H_2SO_4. The absorbance was measured using an Anthos 2020 microplate reader (Biochrom Ltd., Cambridge, UK) at 492 nm, and the OD values of the untreated cells were subtracted from those of the treated cells.

2.5. TaqMan Low-Density Array (TLDA)

Cells were treated with $ZnCl_2$ for 4 or 24 h, and relative gene expression was measured. In a parallel experiment, cells were pre-treated with $ZnCl_2$ for 24 h and then UVB irradiated. Six hours after exposure, total RNA was isolated using Trizol Reagent (MRC Inc., Cincinnati, Ohio, USA), and total RNA was quantified using a Nanodrop 2000 (Thermo Fisher Scientific, Wilmington, USA). cDNA was then synthesised using the High-Capacity cDNA Reverse

Transcription kit (Applied Biosystems, Foster City, CA, USA) according to the manufacturer's instructions. We designed Custom TaqMan Array Microfluidic Cards (384-well) by first selecting 91 genes based on their roles connected to zinc and the UVB response. The selected genes were involved in cell cycle progression, inflammation, apoptosis, DNA repair, and antioxidant defence (Supplementary 1). Genes connected with zinc homeostasis and some with an identified MRE in the promoter region were also added. The TLDA was performed using an Applied Biosystems 7900HT Real-Time PCR System according to the manufacturer's protocol. cDNA (100 ng) in 100 μL of 1X Taqman Gene Expression Master Mix (Applied Biosystems, Foster City, CA, USA) was loaded into each port of the TLDA plates, and each sample was examined in pairs. The PCR program used for amplification was as follows: 94°C for 1 min; 40 cycles of 94°C for 12 sec; and 60°C for 45 sec. The data were derived from three independently performed experiments and were analysed using SDS 2.1 software. ACTB, GAPDH, SDHA, and PGK1 were used for normalisation. Relative gene expression values were calculated using the 2^{-ddCt} method [21, 22].

2.6. Measurement of superoxide ($O_2^{\bullet-}$) production

After 4 or 24 h of $ZnCl_2$ treatment or after 24 h of $ZnCl_2$ treatment combined with UVB, the production of $O_2^{\bullet-}$ was measured using a dihydroethidium (HE) assay (Sigma-Aldrich, St. Louis, MO, USA) 1, 4, 10, and 24 h after UVB exposure. A working solution of HE at a 2 μM final concentration was added to the cells and then incubated for 30 min at 37°C. The cells were then harvested, and the fluorescence intensity was measured by flow cytometry with a FACSCalibur (BD Biosciences, San Jose, USA) to determine the fluorescence intensity at 450 nM, with 620 nm as a reference. The production of $O_2^{\bullet-}$ was expressed as the mean of HE-fluorescence intensity [23].

2.7. Detection of hydrogen peroxide

After 4, 10 or 24 h of $ZnCl_2$ treatment, hydrogen peroxide production was determined using an Amplex red (10-acetyl-3,7-dihydroxyphenoxazine) assay. In this assay, a working solution of Amplex Red (Invitrogen, Eugene, Oregon, USA) at a 50-μM final concentration and horseradish peroxidase (Sigma-Aldrich, St. Louis, MO, USA) at a 0.1 U/ml final concentration was added to the cells and then incubated for 20 min at room temperature. Fluorescence was subsequently read, with excitation at 530 nm and emission at 590 nm, using

a Fluoroskan Ascent FL plate reader (Thermo Scientific, Vantaa, Finland). The MFI values of untreated cells were subtracted from those of the treated cells.

2.9. Western blotting

Cells were treated with $ZnCl_2$ for 4, 24, 48 or 72 h and lysed in RIPA buffer (Sigma-Aldrich, St. Louis, MO, USA). The protein concentration was then estimated using a BCA protein assay kit (Pierce Biotechnology, Rockford, USA). Proteins (20 μg) were separated on 10 or 12% SDS-polyacrylamide gels and then transferred onto nitrocellulose membranes by electroblotting. The membranes were then blocked with 5% low-fat milk in TTBS (0.1% Tween-20 in Tris-buffered saline) or in PBST (0.05% Tween-20 in PBS) and incubated overnight with primary antibody against heme oxygenase-1 (HMOX1) (#ab13248, Abcam Inc., Cambridge, USA) at 1:250 dilution or MTI/II (#ab12228, Abcam Inc., Cambridge, USA) at 1:1000 dilution in 5% milk at 4°C. The membranes were then washed and incubated with horseradish peroxidase-conjugated secondary antibody for 1 h at room temperature. After washing, the signals were visualised using ECL™ Prime Western Blotting Detection Reagent (GE Healthcare, Freiburg, Germany). β-actin (Cell Signaling Technology Inc., Danvers, MA, USA) was used for normalisation.

2.10. Statistics

Statistical analysis was performed using GraphPad Prism Software 5.03 (GraphPAD Software Inc., San Diego, CA, USA), and p values were calculated using a 2-tailed Student's t test. Statistical significance was accepted when $p < 0.05$.

3. Results

3.1. Zn (II) increased cell proliferation

To examine the effect of Zn (II) exposure on cell proliferation, HaCaT cells were treated with Zn (II) at concentrations of 50 and 100 µM in growth medium containing 10% FBS, and the effects were measured using an EZ4U assay. We found that 72-h treatment with 100 µM Zn (II) resulted in significantly increased cell proliferation (1.3-fold; p=0.045) (Figure 1).

3.2. Zn (II) exposure impacted the expression of genes involved in zinc homeostasis, antioxidant defence, cell viability and inflammation in HaCaT cells

Then, we identified genes that showed altered expression in response to 100 µM Zn (II)-containing medium using TaqMan Low-Density Array analysis. We detected six significantly up-regulated genes with relative expression levels of at least 1.5-fold in Zn (II)-treated cells compared to the untreated controls (Table 1). The MT1F gene showed the highest overexpression at both time points following Zn (II) treatment (40.86-fold at 4 h; 12.92-fold at 24 h), and MT1X and HMOX1 were expressed more than 10-fold higher in treated cells after 4 h of Zn (II) exposure. The expression levels of MT1E, MT2A and SLC30A1 also showed at least a 2-fold significant difference between treated and untreated cells at both treatment times. The notch homolog 1, translocation-associated (*Drosophila*) (NOTCH1) gene was slightly up-regulated (1.47-fold), and we detected slight but significant suppression of IL8, prostaglandin-endoperoxide synthase 2 (PTGS2), and cytochrome P450 1B1 (CYP1B1) mRNA expression (0.63-fold, 0.68-fold, and 0.63-fold, respectively) after 4 h of Zn (II) treatment. Specific commercial antibodies against MT protein isoforms are not currently available, and the composite of MTI/II can only be investigated at the protein level. Western blot analysis demonstrated that Zn (II) treatment induced the production of MTI/II proteins with a maximum at 48 h (Figure 2a).

3.3. Zn (II) exposure impacted the expression of HMOX1 and induced significant $O_2^{\bullet-}$ production

We also measured the protein expression of HMOX1 after 4 and 24 h of Zn (II) exposure (Figure 2b). Western blot analysis demonstrated that 4-h Zn (II) treatment induced the production of a 34-kDa HMOX1 protein.

On the other hand, the induction of the antioxidant defence protein HMOX1 upon Zn (II) exposure prompted us to examine whether Zn (II) treatment can induce reactive oxygen species. We measured the generation of $O_2^{\bullet-}$ in response to Zn (II) exposure in cells using a flow cytometry-based HE assay. Our data showed significant production of $O_2^{\bullet-}$ after 4 h of Zn (II) treatment compared to the control (p=0.006) (Figure 3a). To further confirm our data, we investigated $O_2^{\bullet-}$ dismutation by measuring the production of H_2O_2, and we found extracellular diffusion of H_2O_2 to the growth medium 24 h after Zn (II) treatment (p=0.019) (Figure 3b).

3.4. Zn (II) pre-exposure decreased the amount of CPDs but enhanced UVB-induced $O_2^{\bullet-}$ generation

To shed light on the mechanism of the zinc-mediated component of the UVB response, we characterised UVB-induced $O_2^{\bullet-}$ generation and CPD formation after 24-h Zn (II) pre-treatment. We examined the level of $O_2^{\bullet-}$ in Zn (II) pre-treated, UVB-irradiated cells and in cells only exposed to UVB (Figure 3c). We observed an increase in $O_2^{\bullet-}$ generation, with a significant plateau 10 h post-UVB irradiation compared to the control (p<0.001), and we detected a time-dependent decrease in the amount of CPDs after UVB irradiation. Zn (II) pre-treatment changed both processes that were induced by UVB (Figure 3d). Our results showed that significantly less CPDs (by 19.64%) were detected 3 h after UVB irradiation in cells pre-treated with Zn (II) for 24 h compared to cells exposed only to UVB (p=0.0082). However, at 10 h post-UVB exposure, significant enhancement of superoxide generation was observed when comparing Zn (II) pre-treated, UVB-irradiated cells to cells only treated with UVB irradiation (p<0.001).

3.5. Zn (II) pre-exposure altered the type of cell death after UVB irradiation, without influencing the overall survival

To investigate the effect of reduced levels of CPDs but elevated $O_2^{\bullet-}$ levels after Zn (II) pre-treatment, flow cytometric apoptosis and EZ4U cell viability assays were used. We found that the cell survival did not change between Zn (II)-treated and control cells 24 h after UVB

irradiation (Figure 4a). Regarding control cells, the percentage of proliferating cells was 88.69% and the viability of cells after UVB irradiation was decreased by 51.96%. Regarding Zn (II) exposure the percentage of proliferating cells was 91.71%, and Zn (II) pre-treatment did not impact the effect of UVB irradiation, the viability of cells was decreased by 50.64% (Figure 4b). On the other hand, Zn (II) pre-treatment significantly decreased the proportion of early apoptotic cells (Annexin V^+PI^-; by 5.94%, 0.57-fold change, p=0.0286) and significantly increased the population of late apoptotic plus necrotic cells (Annexin V^+PI^+ and Annexin V^-PI^+; by 4.61%, 1.12-fold change, p=0.0026) (Figure 4b).

3.6. Zn (II) caused a transcriptional shift in the UVB-modulated expression of genes

To determine the molecular mechanism behind the cellular response to the combined effects of Zn (II) and UVB exposure, we performed a TaqMan Low-Density Array analysis to characterise the gene expression changes in HaCaT cells pre-treated with Zn (II). We identified 39 differentially expressed genes in cells only submitted to UVB irradiation 6 h after exposure compared to non-irradiated control cells (Table 2; Supplementary 2). Twelve genes were expressed more than 2-fold higher in UVB-irradiated cells than in control cells, and TNF, PTGS2, and IL-8 showed the highest overexpression (>10-fold). We identified 27 genes that were down-regulated in UVB-irradiated cells compared to the control cells; MT1E was the most repressed (0.12-fold). Furthermore, MTF1 levels were significantly decreased compared to the control (0.32-fold). We observed a modest modulation in gene expression when comparing Zn (II) pre-treated, UVB-irradiated cells to those that were only UVB-irradiated. Zn (II) pre-exposure mainly reduced UVB-induced HIPK2 mRNA suppression and caused little modification of POLB and RAD51 mRNA levels, whose relative gene expression levels were repressed following UVB irradiation (<0.75-fold) but remained unchanged (0.76–1.5-fold change) when pre-treated with Zn (II).

4. Discussion

The events involved in the regulation of zinc homeostasis are complex and incompletely understood [24]. In the skin, zinc is related to physiological functions, as shown from the consequences of zinc deficiency [1, 2]. The use of zinc-containing topical therapeutics is widespread due to its clear benefit on cutaneous regeneration and on various inflammatory skin conditions [3]. UVB, the main harmful environmental factor in skin, induces intracellular zinc release in keratinocytes, suggesting a functional role of zinc in the UV stress response [15, 16].

Extracellular zinc is thought to enter the cell through plasma membrane zinc importers and then is transported via a muffler with high affinity for zinc (e.g., MT) to intracellular storage sites such as the endoplasmic reticulum [25]. Passive diffusion of zinc across cell membranes is not possible [26]. Bozym et al. [27] investigated the effect of cell culture medium on the intracellular Zn (II) concentration and found that both the type of cell and the medium influence the intracellular free Zn (II) level during exposure to a certain concentration of Zn (II) and that the toxicity of supplemented Zn (II) must be carefully investigated. Previous experiments have shown that the exposure of HaCaT keratinocytes to 100 μM $ZnCl_2$ was non-toxic to the skin cells [28], and we have not found this concentration to be toxic in our experimental conditions. Based on the calculations of Bozym et al. [27], 100 μM Zn (II) treatment leads to an approximate 100-nM increase of intracellular Zn (II). We also investigated the mRNA expression of MT isoforms. More than 10 functional MT isoforms are present in humans and are classified into four groups; we analysed the mRNA expression of nine of the MT isoforms from the MT1 and MT2 groups in keratinocytes in our experiments [29]. We detected the expression of four isoforms, namely MT2A, MT1X, MT1E, and MT1F. Zn (II) treatment significantly increased the mRNA expression of all four MT isoforms and SLC30A1 (Table 1.). Specific antibodies against the MT protein isoforms are not available; therefore, a composite of MTI/II can only be investigated at the protein level. Western blot analysis demonstrated that Zn (II) treatment induced the production of MTI/II protein in a time-dependent manner (Figure 2a). In addition, we investigated the cellular localisation of MTs and found that MTs were present mostly in the nuclei of control cells, but after 24 h of treatment with Zn (II), we detected high amounts of MTs in the cytoplasm of the cells (data not shown). The variability of the localisation of MTs upon Zn (II) exposure may reflect the expression of MT isoforms with distinct function. Previously, we found high MTI/II protein expression in the nuclei of benign nevus cells, while high levels of MTI/II were present also

in the cytoplasm of cells in malignant melanoma [10]. In the present study we found a significant proliferation advantage upon 100 μM $ZnCl_2$ exposure, in accordance with a previous study [28]. We also tested the effect of 50 μM $ZnCl_2$ treatment, but the change in proliferation was not significant. Although the effects of zinc on intracellular signalling events are not completely known, a positive impact of Zn (II) on cell proliferation might be attributed, at least in part, to the inhibition of phosphatases, leading to augmented protein tyrosine phosphorylation [30]. The proliferation advantage by Zn (II) treatment can also be a consequence of increased calcium uptake [31] or up-regulated gene expression (e.g., NOTCH1, *see* Table 1) [32,33]. Interestingly, in aged skin, which is characterised by decreased epidermal renewal, the expression of MT is lower [34].

The mechanism of action of zinc impact on cell signalling is not well understood [25]; herein, we found that zinc might affect reactive oxygen species (ROS)-sensitive signalling pathways. This is the first report demonstrating high expression of HMOX1 in cultured human keratinocytes upon nontoxic Zn (II) exposure (Figure 2b). The HMOX1 gene encodes an important member of the phase-II enzymes, which have cytoprotective roles in ROS scavenging. Furthermore, HMOX1 was shown to prevent cell death and to have a role in the regulation of inflammation [35-37]. Nontoxic generation of $O_2^{\bullet-}$ with subsequent H_2O_2 release was detected during nontoxic Zn (II) exposure (Figure 3a and 3b) and could explain the HMOX1 expression. Although Zn (II) itself is reported to be an inducer of oxidative stress by promoting mitochondrial and extra-mitochondrial production of ROS [15], the generation of ROS at a nontoxic level upon Zn (II) exposure/release has not been described. Nevertheless, $O2^{\bullet-}$-producing NAD(P)H oxidases are activated in response to growth factors and oncogenes, and enhanced cell proliferation was observed upon ROS-inducing, low-dose photodynamic treatment [38-42]. Therefore, simultaneous increases in cell proliferation and ROS levels are not conflicting. In addition, NADPH oxidase mediated the induction of NFκB and HMOX1 in human colon cancer cells [43] without inducing cell death. Furthermore, the immune response can be redox-regulated [44], and we have observed down-regulation of some pro-inflammatory mediators, such as IL8 and PTGS2, which are partly regulated by redox-sensitive transcription factors (e.g., AP-1) [45].

UVB exposure is the primary risk factor in skin-tumour development [46]. A role of zinc in the mechanism of UVB-induced cell death has already been proposed. Stork et al. [15] described that the elevation of intracellular zinc levels after UVB irradiation is proportional to the fraction of dying or dead cells, and they concluded that UVB-induced zinc release may be an important step in UVB-induced cell death pathways. The consequences of UVB-induced

direct (primarily CPDs) and indirect (free radical generation) DNA damage are cell cycle arrest, DNA repair, and the induction of cell death pathways causing sunburn, inflammation, immunosuppression, and melanogenesis in the skin [47]. We measured both the CPD level and superoxide generation (Figure 3c and 3d). Due to DNA repair processes, the amount of CPDs was decreased with time, and cells with unrepaired DNA damage were eliminated by apoptosis (Figure 4b). Similar to the results of Saito et al., pre-treatment of cells with Zn (II) for 24 h was not sufficient to improve cell survival (Figure 4a), although the level of induced CPD was lower in these cells 3 h after UVB irradiation [48]. We assume that MT could exert some effect on CPD formation because partial translocation of MTs to the nucleus was observed 3 h after UVB irradiation (data not shown). Nevertheless, when further analysing cell death at 24 h post-UVB irradiation, when UVB-induced apoptosis is maximal [49], we found that the fraction of early apoptotic cells decreased, while the fraction of late apoptotic plus necrotic cells increased in Zn (II) pre-treated cells (Figure 4b). In the context of our results, the elevation of intracellular zinc levels after UVB irradiation that was described by Stork et al. was proportional to the fraction of dying or dead cells [15]. When investigating the course of ROS production, the increase in superoxide production upon UVB treatment occurred at a maximum of 10 h, but unexpectedly, this was augmented by Zn (II) pre-exposure (Figure 3c). It has recently been described that a vicious circle of ROS-induced zinc release and zinc-driven mitochondrial ROS production is an important neuronal cell death mechanism [50]. On the other hand, it has been reported that the induction of a type of cell death other than apoptosis in cancer cells might increase the immunogenic potential of cell death [51, 52]. Whether a change in the death process upon Zn (II) pre-exposure can affect the immune response to UV-damaged cells, which would impact the development of various pathologies, e.g., autoimmunity or cancers, must be further studied.

Zinc is redox inert metal. Observed changes in ROS might be attributed to the molecular effects of Zn (II) interactions with cysteinyl thiols, which alters protein functionality and thereby their reactivity and participation in redox reactions [8]. It seems worthy to further examine the role of zinc in skin because further clarification of this issue can affect our thinking about the pathogenesis of skin diseases and can help identify new therapeutic targets.
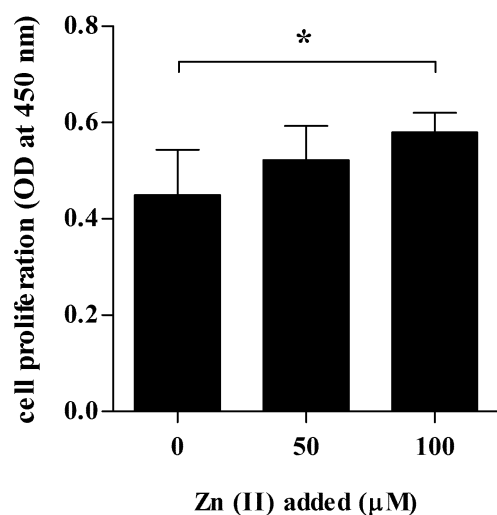
Figure 1. Effect of Zn (II) exposure on cell proliferation in HaCaT keratinocytes.

HaCaT cells were treated with 50 or 100 μM ZnCl$_2$ for 72 h, and cell proliferation was measured by an EZ4U assay. The data were derived from three independent experiments and are presented as the mean ± SEM. An asterisk indicates a significant difference between ZnCl$_2$-treated and control cells at $p < 0.05$, with a 2-tailed Student's t test.
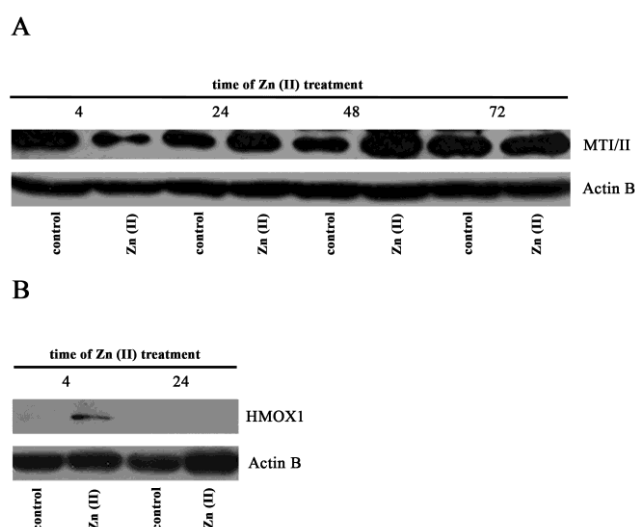

Figure 2. Effect of Zn (II) exposure on the protein expression of MTI/II and HMOX1

HaCaT cells were treated with 100 μM ZnCl$_2$ for 4, 24, 48 or 72 h, and western blotting **A** for MTI/II and **B** for HMOX1 were performed. Actin B protein expression was used as a reference; the representative data of three independent experiments are shown.
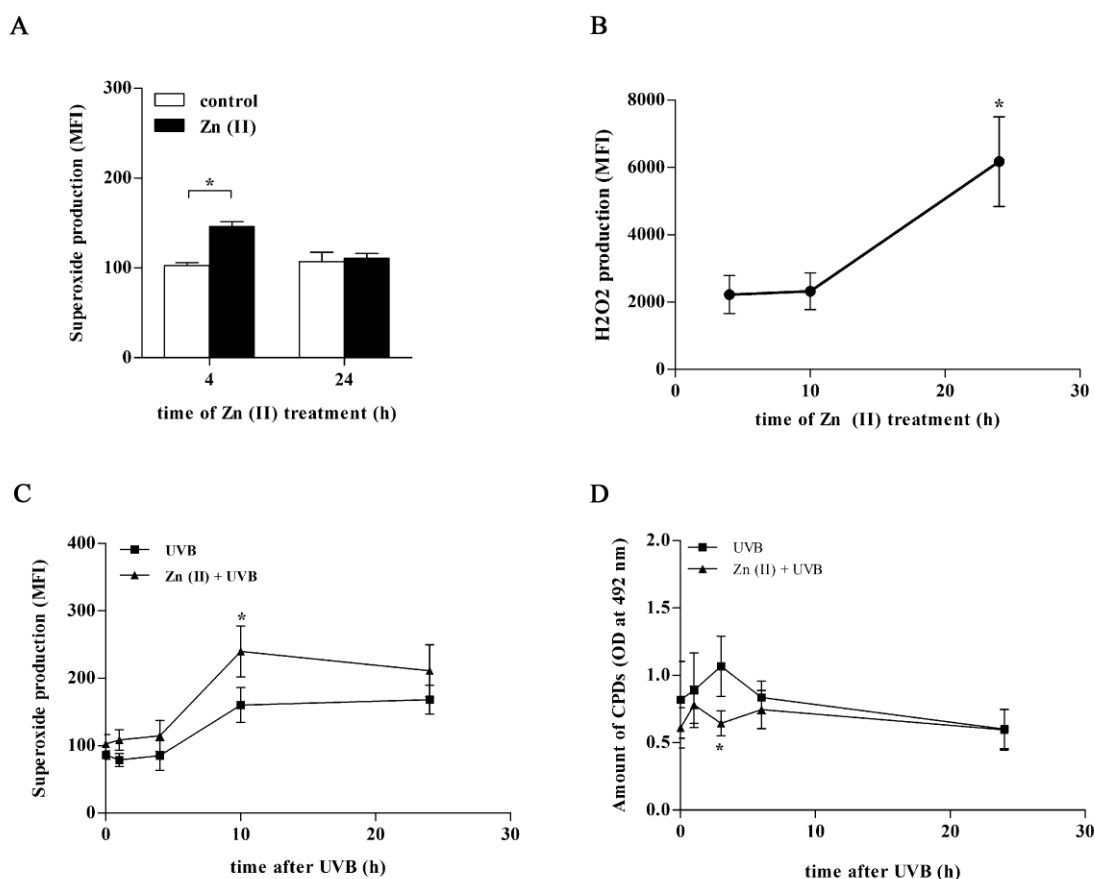
Figure 3. Effect of Zn (II) exposure on the production of reactive oxygen species and on the UVB-induced DNA-damage response

HaCaT cells were treated with 100 μM ZnCl$_2$ for 4 or 24 h and **A** the production of O$_2^{\bullet-}$ was analysed using a flow cytometry-based dihydroethidium assay. **B** Cells were exposed to 100 μM ZnCl$_2$ for 4, 10 or 24 h, and the production of H$_2$O$_2$ was measured using a fluorimetric-based Amplex Red assay. The MFI values of untreated cells were subtracted from those of the treated cells. **C** HaCaT cells were treated with 100 μM ZnCl$_2$ for 24 h followed by 20 mJ/cm^2 UVB irradiation, and the amount of CPDs was determined at 0, 1, 3, 6, and 24 h after UVB irradiation using a CPD-specific ELISA. The OD values of untreated cells were subtracted from those of the treated cells. **D** The production of O$_2^{\bullet-}$ was measured by a flow cytometry-based dihydroethidium assay 1, 4, 10, and 24 h after UVB treatment.

The data were derived from three independent experiments and are presented as the mean ± SEM. An asterisk indicates a significant difference between ZnCl$_2$-treated and control cells (**A, B**) or between the ZnCl$_2$ and UVB combination treatment and cells only exposed to UVB (**C, D**) at $p < 0.05$, using a 2-tailed Student's t test.

A
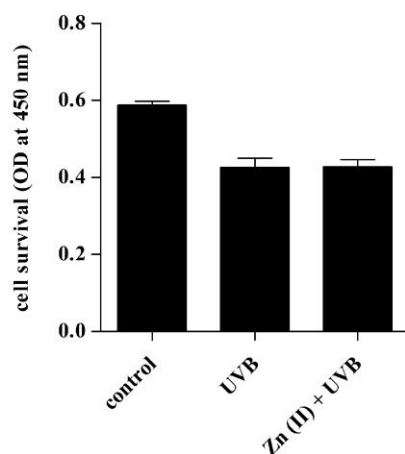
B
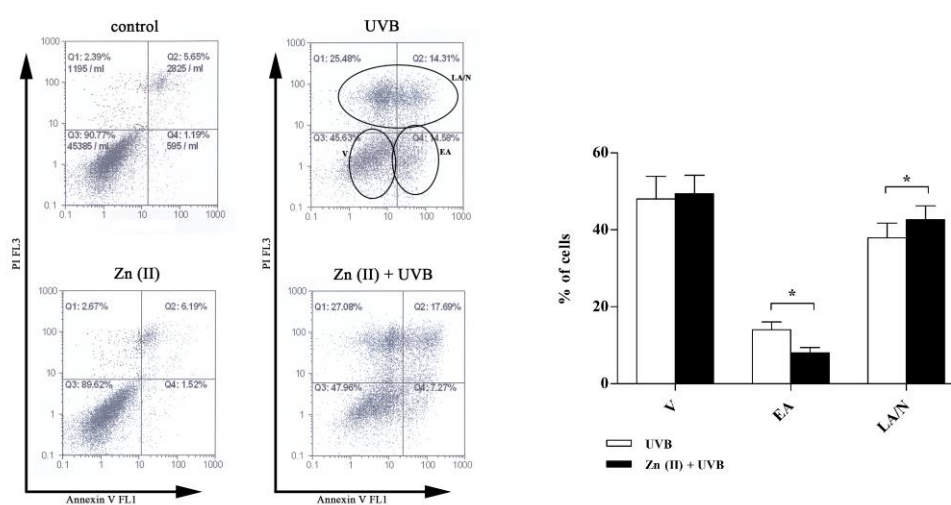
Figure 4. Effect of Zn (II) exposure on the UVB-induced cell death

HaCaT cells were treated with 100 μM ZnCl$_2$ for 24 h followed by 20 mJ/cm^2 UVB irradiation, and **A** cell survival was measured using an EZ4U assay 24 h after UVB. **B** The rate of apoptosis was investigated by flow cytometry using Annexin V and propidium iodide staining 24 h after UVB irradiation. V=viability; EA=early apoptosis; LA/N=late apoptosis plus necrosis. The data were derived from three independent experiments and are presented as the mean ± SEM, p values were calculated by 2-tailed Student's t test.

Gene Symbol	fold change (2^{-ddCt})	
	4 h after Zn (II) treatment	24 h after Zn (II) treatment
MT1F	**40.86**	**12.92**
MT1X	**17.34**	**3.24**
HMOX1	**15.33**	**1.56**
MT1E	**7.30**	**2.12**
MT2A	**6.44**	**3.03**
SLC30A1	**6.41**	**2.48**
NOTCH1	**1.47**	1.06
PTGS2	**0.68**	1.01
IL8	**0.63**	0.92
CYP1B1	**0.63**	1.32

Table 1. Differentially expressed genes upon Zn (II) treatment

The relative gene expression of the listed genes was measured in HaCaT cells treated with 100 μM ZnCl$_2$ relative to untreated cells by TLDA. Values greater than 1.5 but less than 0.75 are highlighted in bold and indicate significant t-test results at $p < 0.05$, using a 2-tailed Student's t test.

	fold change (2^{-ddCt})	
	4 h after Zn (II) treatment	24 h after Zn (II) treatment

fold change (2^{-ddCt})		UVB				
		≤ 0.5	≥ 2	0.55 - 0.75	1.5 - 2	0.76 – 1.5 /not significantly different from control*
Zn (II) + UVB	≤ 0.5	APC MSH6 ATM MT1E ATR MTF1 BCL2 NOTCH1 BCL2L1 RAD52 CCNF SKIL CHEK2 TP73 ERCC3 TRIM26 ERCC4 VEGFC IGF1R XPC ITCH XRCC2 MDM2 XRCC3 MSH2				
	≥ 2		CCNE1 IL8 CDKN1A JUN FOS PTGS2 GADD45B SNAI2 HBEGF TNF IL1B ATF3			MT1F MT1X MT2A SLC30A1
	0.55 – 0.75	ERCC5		CHEK1 ERCC2 SMUG1 TREX1		
	1.5 - 2				CEBPA CYP1A1 DDIT3	
	0.76 - 1.5 /not significantly different from control*	HIPK2		DDB2 NTHL1 POLB RAD51		

Table 2. Effect of Zn (II) pre-treatment on transcriptional changes induced by UVB irradiation

Relative gene expression was measured 6 h after UVB irradiation in HaCaT cells exposed to 20 mJ/cm^2 UVB or pre-treated with 100 μM ZnCl$_2$ for 24 h and then UVB irradiated relative to untreated cells, using TLDA.

Metallomics

Gene Symbol	Assay ID	Gene Name
ACTB[l]	Hs99999903_m1	actin, beta
AKT1 [b]	Hs00178289_m1	v-akt murine thymoma viral oncogene homolog 1
APC [b]	Hs01568269_m1	Adenomatous Polyposis Coli
APEX [d]	Hs00172396_m1	APEX nuclease (multifunctional DNA repair enzyme) 1
ATF3[a, b]	Hs00231069_m1	activating transcription factor 3
ATM [b]	Hs01112307_m1	ataxia telangiectasia mutated
ATR [b]	Hs00354807_m1	ataxia telangiectasia and Rad3 related
BAD [b]	Hs00188930_m1	BCL2-associated agonist of cell death
BCL2 [b]	Hs00608023_m1	B-cell CLL/lymphoma 2
BCL2L1 [b]	Hs00236329_m1	BCL2-like 1
C11orf31[h,i]	Hs00415057_m1	chromosome 11 open reading frame 31
CCNE1 [b]	Hs01026536_m1	cyclin E1
CCNF [b]	Hs00171049_m1	cyclin F
CDKN1A [b]	Hs00355782_m1	cyclin-dependent kinase inhibitor 1A (p21, Cip1)
CEBPA [b, h]	Hs00269972_s1	CCAAT/enhancer binding protein (C/EBP), alpha
CEBPB [b]	Hs00270923_s1	CCAAT/enhancer binding protein (C/EBP), beta
CHEK1 [b]	Hs00967506_m1	CHK1 checkpoint homolog (S. pombe)
CHEK2 [b]	Hs00200485_m1	CHK2 checkpoint homolog (S. pombe)
CYP1A1 [k]	Hs00153120_m1	cytochrome P450, family 1, subfamily A, polypeptide 1
CYP1B1 [k]	Hs00164383_m1	cytochrome P450, family 1, subfamily B, polypeptide 1
DDB1 [c]	Hs00172410_m1	damage-specific DNA binding protein 1, 127kDa

DDB2 [c]	Hs03044953_m1	damage-specific DNA binding protein 2, 48kDa
DDIT3 [b]	Hs01090850_m1	DNA-damage-inducible transcript 3
ERCC1 [c]	Hs01012158_m1	excision repair cross-complementing rodent repair deficiency, complementation group 1 (includes overlapping antisense sequence)
ERCC2 [c]	Hs00361161_m1	excision repair cross-complementing rodent repair deficiency, complementation group 2
ERCC3 [c]	Hs01554450_m1	excision repair cross-complementing rodent repair deficiency, complementation group 3 (xeroderma pigmentosum group B complementing)
ERCC4 [c]	Hs00193342_m1	excision repair cross-complementing rodent repair deficiency, complementation group 4
ERCC5 [c]	Hs00164482_m1	excision repair cross-complementing rodent repair deficiency, complementation group 5
FOS [b]	Hs00170630_m1	FBJ murine osteosarcoma viral oncogene homolog
GADD45B [b]	Hs00169587_m1	growth arrest and DNA-damage-inducible, beta
GAPDH [l]	Hs99999905_m1	glyceraldehyde-3-phosphate dehydrogenase
GLI1 [j]	**Hs01110766_m1**	**GLI family Zinc (II) finger 1**
HBEGF [a, b]	Hs00181813_m1	heparin-binding EGF-like growth factor
HIPK2 [b]	Hs00179759_m1	homeodomain interacting protein kinase 2
HMOX1 [i]	Hs01110250_m1	heme oxygenase (decycling) 1
HSPA6 [k]	**Hs00275682_s1**	**heat shock 70kDa protein 6 (HSP70B')**
HSPD1 [k]	Hs01941522_u1	heat shock 60kDa protein 1 (chaperonin)
IGF1R [b]	Hs00609566_m1	insulin-like growth factor 1 receptor
IL10 [a]	**Hs00961622_m1**	**interleukin 10**
IL1B [a]	Hs01555410_m1	interleukin 1, beta
IL1RN [a]	Hs00893626_m1	interleukin 1 receptor antagonist
IL8 [a]	Hs00174103_m1	interleukin 8
ITCH [b]	Hs00395201_m1	itchy E3 ubiquitin protein ligase homolog (mouse)
JUN [b]	Hs00277190_s1	jun proto-oncogene
KRT10 [j]	**Hs00166289_m1**	**keratin 10**

Metallomics

LCN2[h,i]	Hs01008571_m1	lipocalin 2
MDM2 [b]	Hs00234753_m1	Mdm2 p53 binding protein homolog (mouse)
MGMT[k]	Hs01037698_m1	O-6-methylguanine-DNA methyltransferase
MMP9[a]	**Hs00234579_m1**	**matrix metallopeptidase 9 (gelatinase B, 92kDa gelatinase, 92kDa type IV collagenase)**
MSH2[e]	Hs00953523_m1	mutS homolog 2, colon cancer, nonpolyposis type 1 (E. coli)
MSH6[e]	Hs00264721_m1	mutS homolog 6 (E. coli)
MT1A[g,h]	**Hs00831826_s1**	**metallothionein 1A**
MT1B[g,h]	**Hs00538861_m1**	**metallothionein 1B**
MT1E[g,h]	Hs01938284_g1	metallothionein 1E
MT1F[g,h]	Hs00744661_sH	metallothionein 1F
MT1G[g,h]	**Hs02578922_Gh**	**metallothionein 1G**
MT1H[g,h]	**Hs00823168_g1**	**metallothionein 1H**
MT1M[g,h]	**Hs00828387_g1**	**metallothionein 1M**
MT1X[g,h]	Hs00745167_sH	metallothionein 1X
MT2A[g,h]	Hs01591333_g1	metallothionein 2A
MTF1[g]	Hs00232306_m1	metal-regulatory transcription factor 1
NOTCH1[h,j]	Hs01062014_m1	notch 1
NTHL1 [d]	Hs00959764_m1	nth endonuclease III-like 1 (E. coli)
OGG1 [d]	Hs00213454_m1	8-oxoguanine DNA glycosylase
PARP1 [d]	Hs00242302_m1	poly (ADP-ribose) polymerase 1
PCNA [c, d, e]	Hs00427214_g1	proliferating cell nuclear antigen
PGK1[l]	Hs00943178_g1	phosphoglycerate kinase 1
POLB [d]	Hs01099715_m1	polymerase (DNA directed), beta
PTGS2[a]	Hs00153133_m1	prostaglandin-endoperoxide synthase 2 (prostaglandin G/H synthase and cyclooxygenase)
RAD23B [c]	Hs00234102_m1	RAD23 homolog B (S. cerevisiae)
RAD51[f]	Hs00153418_m1	RAD51 homolog (RecA homolog, E. coli) (S. cerevisiae)
RAD52[f]	Hs00172536_m1	RAD52 homolog (S. cerevisiae)
RPA1 [c, f]	Hs00161419_m1	replication protein A1, 70kDa
S100A7[a,j]	**Hs00161488_m1**	**S100 calcium binding protein A7**
SDHA[l]	Hs00188166_m1	succinate dehydrogenase complex, subunit A, flavoprotein (Fp)
SKIL [b]	Hs01045418_m1	SKI-like oncogene
SLC30A1[g,h]	Hs00253602_m1	solute carrier family 30 (Zinc (II) transporter), member 1

SMUG1 [d]	Hs00204820_m1	single-strand-selective monofunctional uracil-DNA glycosylase 1
SNAI2 [a]	Hs00950344_m1	snail homolog 2 (Drosophila)
TNF [a]	**Hs00174128_m1**	**tumor necrosis factor**
TNFAIP3 [a]	Hs00234713_m1	tumor necrosis factor, alpha-induced protein 3
TP53 [b]	Hs01034249_m1	tumor protein p53
TP73 [b]	Hs01056230_m1	tumor protein p73
TREX1 [e]	Hs03055245_s1	three prime repair exonuclease 1
TRIM26 [a]	Hs00758189_m1	tripartite motif-containing 26
TXN [i]	Hs01555212_g1	thioredoxin
UNG [d]	Hs00422172_m1	uracil-DNA glycosylase
VEGFC [a]	Hs00153458_m1	vascular endothelial growth factor C
XPA [c]	Hs00166045_m1	xeroderma pigmentosum, complementation group A
XPC [c]	Hs01104206_m1	xeroderma pigmentosum, complementation group C
XRCC1 [d]	Hs00959834_m1	X-ray repair complementing defective repair in Chinese hamster cells 1
XRCC2 [f]	Hs03044154_m1	X-ray repair complementing defective repair in Chinese hamster cells 2
XRCC3 [f]	Hs00193725_m1	X-ray repair complementing defective repair in Chinese hamster cells 3
XRCC6 [f]	Hs00995282_g1	X-ray repair complementing defective repair in Chinese hamster cells 6
ZNRD1 [k]	Hs00205908_m1	Zinc ribbon domain containing 1

Supplementary 1. List of selected genes for TaqMan Low-Density Array analysis

Undetermined genes are highlighted in bold.

[a] Inflammation

[b] DNA-damage response

[c] Nucleotide excision repair

[d] Base excision repair

[e] Mismatch repair

[f] Double strand break repair

[g] Zinc homeostasis

[h] Genes containing MRE sites

[i] Oxidative stress

[j] Keratinocyte proliferation/differentiation, cell survival

[k] Others: ZNRD1, MGMT, HSPA6 (HSP70B), HSPD1 (HSP60), CYP1A1, CYP1B1

[1] Housekeeping genes used for normalisation

Metallomics

Gene Symbol	UVB fold change (2^{-ddCt})	p value[1]	Zinc (II) + UVB fold change (2^{-ddCt})	p value[1]
TNF	28,83	0,05815	24,37	0,014558
PTGS2	19,39	0,052279	18,10	0,004363
IL8	18,26	0,011145	21,04	0,00227
ATF3	9,30	0,026083	10,62	0,020249
JUN[2]	8,68	ns	8,21	0,050386
FOS[2]	6,04	ns	7,10	ns
GADD45B	5,85	0,005414	6,57	0,012406
CDKN1A[2]	4,21	ns	4,11	0,037189
CCNE1	3,67	0,044125	4,56	0,022938
SNAI2[2]	3,04	ns	3,42	0,003713
HBEGF	2,71	0,001709	2,79	0,00898
IL1B[2]	2,53	ns	2,43	0,018241
DDIT3	1,78	ns	1,97	0,044236
CYP1A1	1,62	0,042759	1,76	0,025693
CEBPA	1,61	0,024664	1,66	ns
SLC30A1	1,28	ns	2,94	0,032076
MT1X	1,15	ns	4,33	0,01818
MT2A	1,14	ns	3,89	5,58E-05
MT1F	0,78	ns	21,92	0,000983
DDB2	0,74	0,035138	0,84	ns
ERCC2	0,71	0,002939	0,73	0,041664
NTHL1	0,71	0,031694	0,77	ns
RAD51	0,70	0,013263	0,85	ns
CHEK1	0,64	0,053186	0,72	0,019469
SMUG1	0,60	ns	0,58	0,015714
TREX1	0,59	0,044764	0,64	0,032647
POLB	0,56	0,006388	0,77	ns
CHEK2	0,55	0,014411	0,54	0,024618
ERCC5	0,51	0,040806	0,57	0,014313
MSH2	0,50	0,010779	0,54	0,004747
ERCC4	0,50	0,013892	0,55	0,000433
ERCC3	0,49	0,017928	0,48	0,003888
XRCC3	0,46	0,009467	0,46	0,00588
HIPK2	0,46	0,015698	0,74	ns
ITCH	0,45	0,005814	0,47	0,00756
TRIM26	0,42	0,001248	0,47	0,000815
ATM	0,41	0,009832	0,44	0,000551
IGF1R	0,38	0,005486	0,39	0,000444
XPC	0,37	0,002325	0,40	0,005501
BCL2L1	0,36	0,00826	0,37	0,008226
ATR	0,36	0,005014	0,38	0,001731

MSH6	0,35	0,000764	0,41	0,011031
RAD52	0,33	0,001544	0,39	0,00087
MTF1	0,32	0,013172	0,33	0,00492
MDM2	0,30	0,00186	0,33	0,001146
TP73	0,28	0,005793	0,25	0,001074
VEGFC	0,27	0,003256	0,27	0,001116
XRCC2	0,25	0,001383	0,26	0,000498
NOTCH1	0,23	0,001808	0,26	0,000788
SKIL	0,23	0,001938	0,27	0,000269
APC	0,20	0,007314	0,20	0,006341
BCL2	0,18	0,000877	0,12	0,002252
CCNF	0,17	0,000928	0,21	0,001193
MT1E	0,12	0,000225	0,30	0,002777

Supplementary 2. Effect of Zn (II) pre-treatment on transcriptional changes induced by UVB irradiation

The relative gene expression in HaCaT cells exposed to 20 mJ/cm^2 UVB for 6 h or pre-treated with 100 μM $ZnCl_2$ for 24 h and then UVB irradiated was measured and analysed by TLDA relative to untreated cells.

ns, not significant $p < 0.05$

[1] with 2-tailed Student's t test

[2] at least ±2-fold differences in each experiment between treated and untreated cells

References

1. T. Kawamura, Y. Ogawa, Y. Nakamura, S. Nakamizo, Y. Ohta, H. Nakano, K. Kabashima, I. Katayama, S. Koizumi, T. Kodama, A. Nakao and S. Shimada, *J Clin Invest*, 2012, 122, 722-732.
2. B. Portnoy and M. Molokhia, *Lancet*, 1974, 2, 663-664.
3. J. R. Schwartz, R. G. Marsh and Z. D. Draelos, *Dermatol Surg*, 2005, 31, 837-847; discussion 847.
4. M. Gupta, V. K. Mahajan, K. S. Mehta and P. S. Chauhan, *Dermatol Res Pract*, 2014, 2014, 709152.
5. M. M. Molokhia and B. Portnoy, *Br J Dermatol*, 1970, 82, 254-255.
6. B. L. Vallee and K. H. Falchuk, *Physiol Rev*, 1993, 73, 79-118.
7. L. A. Lichten and R. J. Cousins, *Annu Rev Nutr*, 2009, 29, 153-176.
8. W. Maret, *J Nutr*, 2000, 130, 1455S-1458S.
9. A. Zamirska, L. Matusiak, P. Dziegiel, G. Szybejko-Machaj and J. C. Szepietowski, *Pathol Oncol Res*, 2012, 18, 849-855.
10. E. Emri, K. Egervari, T. Varvolgyi, D. Rozsa, E. Miko, B. Dezso, I. Veres, G. Mehes, G. Emri and E. Remenyik, *J Eur Acad Dermatol Venereol*, 2013, 27, e320-327.
11. T. G. Polefka, R. J. Bianchini and S. Shapiro, *Int J Cosmet Sci*, 2012, 34, 416-423.
12. B. W. Graf, E. J. Chaney, M. Marjanovic, M. De Lisio, M. C. Valero, M. D. Boppart and S. A. Boppart, *Biomed Opt Express*, 2013, 4, 1817-1828.
13. C. C. Wang, S. Wang, Q. Xia, W. He, J. J. Yin, P. P. Fu and J. H. Li, *J Nanosci Nanotechnol*, 2013, 13, 3880-3888.
14. S. D. Lamore, C. M. Cabello and G. T. Wondrak, *Cell Stress Chaperones*, 2010, 15, 309-322.
15. C. J. Stork, L. M. Martorano and Y. V. Li, *Int J Mol Med*, 2010, 26, 463-469.
16. L. Wang, W. Liu, S. H. Parker and S. Wu, *Life Sci*, 2010, 86, 448-454.
17. W. H. Wang, L. F. Li, B. X. Zhang and X. Y. Lu, *Clin Exp Dermatol*, 2004, 29, 57-61.
18. E. Jourdan, N. Emonet-Piccardi, C. Didier, J. C. Beani, A. Favier and M. J. Richard, *Arch Biochem Biophys*, 2002, 405, 170-177.
19. E. Jourdan, R. Marie Jeanne, S. Regine and G. Pascale, *J Cell Biochem*, 2004, 92, 631-640.
20. M. O. Parat, M. J. Richard, S. Pollet, C. Hadjur, A. Favier and J. C. Beani, *J Photochem Photobiol B*, 1997, 37, 101-106.
21. T. D. Schmittgen and B. A. Zakrajsek, *J Biochem Biophys Methods*, 2000, 46, 69-81.
22. J. Winer, C. K. Jung, I. Shackel and P. M. Williams, *Anal Biochem*, 1999, 270, 41-49.
23. M. Szanto, I. Rutkai, C. Hegedus, A. Czikora, M. Rozsahegyi, B. Kiss, L. Virag, P. Gergely, A. Toth and P. Bai, *Cardiovasc Res*, 2011, 92, 430-438.
24. P. I. Oteiza, *Free Radic Biol Med*, 2012, 53, 1748-1759.
25. K. M. Taylor, P. Kille and C. Hogstrand, *Cell Cycle*, 2012, 11, 1863-1864.
26. K. M. Taylor, P. Vichova, N. Jordan, S. Hiscox, R. Hendley and R. I. Nicholson, *Endocrinology*, 2008, 149, 4912-4920.
27. R. A. Bozym, F. Chimienti, L. J. Giblin, G. W. Gross, I. Korichneva, Y. Li, S. Libert, W. Maret, M. Parviz, C. J. Frederickson and R. B. Thompson, *Exp Biol Med (Maywood)*, 2010, 235, 741-750.
28. M. O. Parat, M. J. Richard, C. Meplan, A. Favier and J. C. Beani, *Biol Trace Elem Res*, 1999, 70, 51-68.
29. D. Lim, T. T. Phan, G. W. Yip and B. H. Bay, *Int J Mol Med*, 2006, 17, 385-389.

30. E. Bellomo, A. Massarotti, C. Hogstrand and W. Maret, *Metallomics*, 2014, 6, 1229-1239.
31. B. L. O'Dell and J. D. Browning, *Adv Nutr*, 2013, 4, 287-293.
32. Y. Wang, U. Wimmer, P. Lichtlen, D. Inderbitzin, B. Stieger, P. J. Meier, L. Hunziker, T. Stallmach, R. Forrer, T. Rulicke, O. Georgiev and W. Schaffner, *FASEB J*, 2004, 18, 1071-1079.
33. P. Lichtlen, Y. Wang, T. Belser, O. Georgiev, U. Certa, R. Sack and W. Schaffner, *Nucleic Acids Res*, 2001, 29, 1514-1523.
34. C. Ma, L. F. Li and X. Chen, *Br J Dermatol*, 2011, 164, 479-482.
35. A. M. Bhujade, S. Talmale, N. Kumar, G. Gupta, P. Reddanna, S. K. Das and M. B. Patil, *J Ethnopharmacol*, 2012, 141, 989-996.
36. Y. C. Hseu, C. W. Chou, K. J. Senthil Kumar, K. T. Fu, H. M. Wang, L. S. Hsu, Y. H. Kuo, C. R. Wu, S. C. Chen and H. L. Yang, *Food Chem Toxicol*, 2012, 50, 1245-1255.
37. S. J. Chapple, R. C. Siow and G. E. Mann, *Int J Biochem Cell Biol*, 2012, 44, 1315-1320.
38. A. Blazquez-Castro, T. Breitenbach and P. R. Ogilby, *Photochem Photobiol Sci*, 2014, 13, 1235-1240.
39. A. O. Brightman, J. Wang, R. K. Miu, I. L. Sun, R. Barr, F. L. Crane and D. J. Morre, *Biochim Biophys Acta*, 1992, 1105, 109-117.
40. A. W. Linnane, M. Kios and L. Vitetta, *Biogerontology*, 2007, 8, 445-467.
41. E. Werner, *J Cell Sci*, 2004, 117, 143-153.
42. G. Y. Zhang, L. C. Wu, T. Dai, S. Y. Chen, A. Y. Wang, K. Lin, D. M. Lin, J. Q. Yang, B. Cheng, L. Zhang, W. Y. Gao and Z. J. Li, *Exp Dermatol*, 2014, 23, 639-644.
43. G. S. Lien, M. S. Wu, M. Y. Bien, C. H. Chen, C. H. Lin and B. C. Chen, *PLoS One*, 2014, 9, e104891.
44. M. Valko, D. Leibfritz, J. Moncol, M. T. Cronin, M. Mazur and J. Telser, *Int J Biochem Cell Biol*, 2007, 39, 44-84.
45. Y. J. Surh, J. K. Kundu, H. K. Na and J. S. Lee, *J Nutr*, 2005, 135, 2993S-3001S.
46. F. P. Noonan, J. A. Recio, H. Takayama, P. Duray, M. R. Anver, W. L. Rush, E. C. De Fabo and G. Merlino, *Nature*, 2001, 413, 271-272.
47. L. Marrot and J. R. Meunier, *J Am Acad Dermatol*, 2008, 58, S139-148.
48. T. Saito, T. Tezuka, R. Konno and N. Fujii, *Jpn J Ophthalmol*, 2010, 54, 486-493.
49. D. E. Godar and A. D. Lucas, *Photochem Photobiol*, 1995, 62, 108-113.
50. M. C. McCord and E. Aizenman, *Front Aging Neurosci*, 2014, 6, 77.
51. M. Cirone, A. Garufi, L. Di Renzo, M. Granato, A. Faggioni and G. D'Orazi, *Oncoimmunology*, 2013, 2, e26198.
52. M. Granato, V. Lacconi, M. Peddis, L. V. Lotti, L. Di Renzo, R. Gonnella, R. Santarelli, P. Trivedi, L. Frati, G. D'Orazi, A. Faggioni and M. Cirone, *Cell Death Dis*, 2013, 4, e730.